Mechanism and Machine Theory 142 (2019) 103598

Contents lists available at ScienceDirect

Mechanism and Machine Theory

journal homepage: www.elsevier.com/locate/mechmachtheory

Research paper

A novel 6R metamorphic mechanism with eight motion branches and multiple furcation points

Yaqing Song[a], Xuesi Ma[a], Jian S Dai[b,*]

[a] MoE Key Laboratory for Mechanism Theory and Equipment Design, International Centre for Advanced Mechanisms and Robotics, School of Mechanical Engineering, Tianjin University, Tianjin 300072, PR China
[b] Chair of Mechanisms and Robotics, Advanced Kinematics and Reconfigurable Robotics Lab, School of Natural and Mathematical Sciences, King's College London, Strand, London WC2R 2LS, United Kingdom

ARTICLE INFO

Article history:
Received 11 May 2019
Revised 16 July 2019
Accepted 13 August 2019

Keywords:
Furcation points
Geometrically constrained
Motion branch
Geometry morphology
Screws

ABSTRACT

The furcation point in a mechanism is a salient feature of reconfigurable mechanisms and change of a joint from an unconstrained condition to a geometrically constrained condition resulting in naturally link annexing with this geometrical constraint is a typical feature of metamorphic mechanisms. This paper presents a novel 6R metamorphic mechanism by inserting two revolute joints to a Bennett mechanism. From parameters of this novel 6R metamorphic mechanism, the source mechanism before changing is a special case of the Bricard 6R line-symmetric mechanism while the closure equation gives constraint conditions of joints. The geometrically constrained conditions result in variable motion branches of the mechanism. When all joints are unconstrained geometrically, two 6R motion branches can be obtained and when two joints are under geometric constrained, three 4R motion branches can be obtained. Further, three further motion branches with coaxial joints are obtained and motion branch transformation is illustrated with kinematic curves. For each of the motion branches, motion screws of this novel 6R metamorphic mechanism present corresponding geometry morphology and are analysed with screw algebra.

1. Introduction

Metamorphic mechanisms were proposed by Dai and Rees Jones [1] in the 1990s. The mechanisms were revealed from origami arts that change their topologies and subsequently the finite mobility with reconfiguration of joints and with link annexing resulting from geometrical constraints. This type of mechanisms can adapt to various work conditions and meet various needs. Kinematotropic mechanisms were revealed by Wohlhart [2] in the same period. He noticed that this type of mechanisms can change their finite mobility when they pass through specific configurations without giving any link annexing. The two types of the mechanisms developed in 1990s became the foundation of reconfigurable mechanisms and created a new field in reconfigurable mechanisms and reconfigurable robotics.

* Corresponding author.
E-mail addresses: yqsong@tju.edu.cn (Y. Song), maxuesi@tju.edu.cn (X. Ma), jian.dai@kcl.ac.uk (J.S. Dai).

https://doi.org/10.1016/j.mechmachtheory.2019.103598

Sugimoto et al. [3] gave a definition of uncertain singularity using screw theory. This gave a foundation for bifurcation of mechanisms. Kieffer [4] used a Taylor expansion of the curve to analyze bifurcation of mechanisms and distinguish the bifurcation point from the isolated point of the mechanisms. Zlatanov et al. [5] presented constraint singularity and Müller [6] investigated the tangent cone when mechanisms are at the singularity point. Qin et al. [7] examined the bifurcation points and investigated a derivative queer-square mechanism for the bifurcation theory by developing the multi-furcation theory of reconfigurable mechanisms. Aimedee et al. [8] further analyzed the way of reconfiguration in reconfigurable mechanisms and presented a systemized method for developing reconfigurable mechanisms.

One type of metamorphic parallel mechanisms investigated by Gan et al. [9] are based on the rT joint. With the invention of the vA joint, Zhang et al. [10] developed another type of metamorphic parallel mechanisms with two 3SvPSv metamorphic parallel mechanisms. Further, Zhang and Dai [11] presented a Bannett plano-spherical reconfigurable linkage with a trifurcation point. For single loop mechanisms, there are many developments into reconfiguration. Song et al. [12] investigated a reconfigurable 6R mechanism with two 6R motion branches and two 4R motion branches. Zhang and Dai [13] developed a new 8R metamorphic mechanism from a kirigami fold with two 6R motion branches. A further evolved Sarrus-motion reconfigurable linkage [14] gave a reconfiguration with a trifurcation point with three different motion branches. Further, a multifurcated 7R mechanisms [15] were developed by Zhang et al. with two 6R motion branches that are geometrically constrained when they go through the furcation points. Chen and Chai [16] gave a reconfigurable 6R mechanism based on the Bricard line-symmetric mechanism and Bricard plane-symmetric mechanism. Feng et al. [17] analyzed the bifurcation behavior of the Bricard plane-symmetric mechanism and gave the corresponding parameters based on the kinematic equation. Chen and You [18] identified the configurations of a 6R mechanism with calculating the state of self-stress of the mechanism. He et al. [19] developed a 7R metamorphic mechanism by adding a revolute joint to the overconstrained Sarrus mechanism. Kong and Pfurner [20] presented an approach to type synthesis of single loop mechanisms with variable DOF by inserting two revolute joints to a planar five-bar mechanism for reconfiguration. Pfurner [21] combined two overconstrained 6R mechanisms to develop a 8R mechanism. Lopez-Custodio et al. [22] proposed a method for generating a metamorphic and reconfigurable mechanism based on the intersection curve of two toroids and investigated a reconfigurable 6R mechanism with two 6R motion branches and two 4R motion branches. Using this method, they produced a reconfigurable mechanism based on the Bricard plane-symmetric mechanism [23].

This paper focuses on a novel 6R metamorphic mechanism with multiple furcation points. First, from an equilateral Bennett mechanism, when two common perpendiculars of a joint axis with its two ajacent joint axes coincide, two joints can then be added this then results in a novel 6R metamorphic mechanism. The design parameters of the 6R metamorphic mechanism and its motion screws are given. Secondly, the closure equation of the 6R metamorphic mechanism are demonstrated. The geometry-constraint conditions of joints determined by the closure equation will be discussed. With different joints conditions, two 6R motion branches, three 4R motion branches and three further motion branches with coaxial joints will be obtained. Further, the geometry morphologies corresponding to different motion branches will be analyzed using motion screws. In this paper, furcation points are given using the relationship of the joint angles and transformation of motion branches will be illustrated with the kinematic curves.

2. The novel 6R metamorphic mechanism derived from a bennett mechanism by using geometric constraint based on D-H parameters

To describe a mechanism, D-H parameters of the links are used as in Fig. 1. $a_{i(i+1)}$ is the link length representing the length of the common normal of axis of joint i and axis of joint $i+1$. $\alpha_{i(i+1)}$ is the twist angle from the axis of joint i to the axis of joint $i+1$ and it is measured about the direction of the common normal from the axis of joint i to the axis of joint $i+1$. θ_i is the angle of a revolute joint from axis x_i to x_{i+1} around joint i. x_i is the direction of common normal form joint i-1 to join i and x_{i+1} is the direction of the common normal from joint i to joint $i+1$. d_i is the distance along the axis

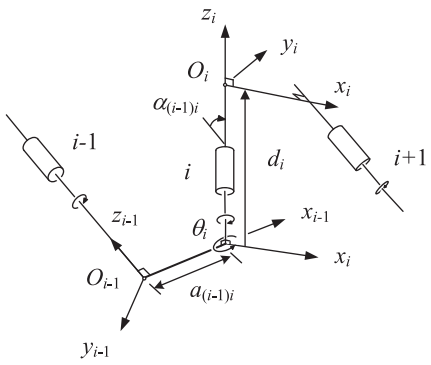

Fig. 1. D-H parameters of the links.

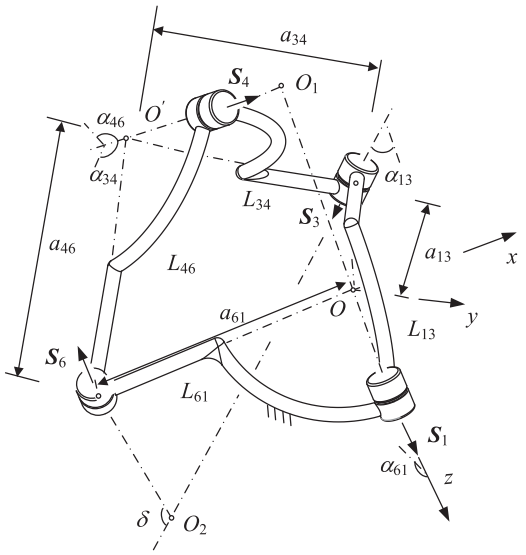

Fig. 2. Original equilateral Bennett mechanism and its D-H parameters.

z from the previous common perpendicular line $a_{(i\text{-}1)i}$ to the current common particular line $a_{i(i+1)}$. z_i is the direction of joint i.

The Bennett mechanism [24,25] is an overconstrained 4R mechanism with its mobility not satisfing the Grübler-Kutabach criterion [26,27]. The original Bennett mechanism is in Fig. 2. O_1 is the intersection point of the axis of joint 1 and the axis of joint 4. O_2 is the intersection point of the axis of joint 3 and the axis of joint 6. For a generic Bennett mechanism, the opposite sides have the same length and twisting angle, and the length and twisting angle of the Bennett mechanism satisfy a certain relation. In order to meet the requirement of diagonal intersection, lengths of four links are identical, as an equilateral Bennett mechanism. $\boldsymbol{S}_i$ is the screw of the axis of joint i and L_{ij} is the link between joint i and joint j. The D-H parameters of the original equilateral Bennett mechanism are

$$\begin{aligned} &\alpha_{13} = \alpha_{46} = \frac{\pi}{4},\ \alpha_{34} = \alpha_{61} = \frac{3\pi}{4} \\ &a_{13} = a_{34} = a_{46} = a_{61} = l \\ &d_1 = d_3 = d_4 = d_6 = 0 \end{aligned} \tag{1}$$

The global coordinate frame is set on link L_{61} as in Fig. 2. z axis is along the axis of joint 1 and x axis is along the common normal of the axis of joint 6 and the axis of joint 1. Origin O is the intersection point of x axis and z axis. y axis is decided by the right-hand rule. In geometrical term, O is the intersection between the common parpendicular of axis of joint 6 with its right ajacent axis of joint 1 and the axis of joint 1. The axis of joint 4 intersects the common normal of the axis of joint 6 and the axis of joint 4 at O'. In geometgrical term, O' is the intersection between the common parpendicular of axis of joint 6 with its left ajacent axis of joint 4 and the axis of joint 4. δ is the angle between the axis of joint 6 and the axis of joint 3.

The screw $\boldsymbol{S}_1$ is

$$\boldsymbol{S}_1 = (0, 0, 1, 0, 0, 0)^{\mathrm{T}} \tag{2}$$

According to Ref. [28], $\boldsymbol{S}_3$ can be obtained using

$$\boldsymbol{S}_3 = \begin{bmatrix} \boldsymbol{R}_{z,\theta_1} & 0 \\ \boldsymbol{R}_{z,\theta_1} & \boldsymbol{R}_{z,\theta_1} \end{bmatrix} \begin{bmatrix} \boldsymbol{R}_{x,\alpha_{13}} & 0 \\ [(a_{13}x)\times]\boldsymbol{R}_{x,\alpha_{13}} & \boldsymbol{R}_{x,\alpha_{13}} \end{bmatrix} (0, 0, 1, 0, 0, 0)^{\mathrm{T}} \tag{3}$$

where $[(a_{13}x)\times]$ is the skew symmetry matrices of $a_{13}x$, $\boldsymbol{x}$ is the unit vector corresponding to x axis, $\boldsymbol{R}_{z,\theta_1}$ is the rotation matrix around z axis and the angle is θ_1, $\boldsymbol{R}_{x,\alpha_{13}}$ is the rotation matrix around x axis and the angle is α_{13}. From Euler-Rodrigues formulas, we have

$$R_{v,\alpha} = \boldsymbol{I} + \sin\alpha[v\times] + (1 - \cos\alpha)[v\times]^2 \tag{4}$$

where $\boldsymbol{I}$ is a 3×3 unit matrix, $[v\times]$ is the skew symmetry matrix of vector $\boldsymbol{v}$, α is the rotation angle. Substituting all the parameters of the Bennett mechanism into Eq. (3), we obtain

$$\boldsymbol{S}_3 = \left(\frac{\sqrt{2}}{2}\sin\theta_1, -\frac{\sqrt{2}}{2}\cos\theta_1, \frac{\sqrt{2}}{2}, \frac{\sqrt{2}}{2}l\sin\theta_1, -\frac{\sqrt{2}}{2}l\cos\theta_1, -\frac{\sqrt{2}}{2}l \right)^{\mathrm{T}} \tag{5}$$

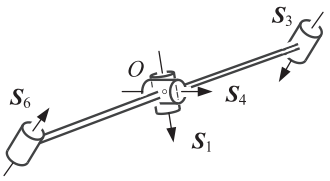

Fig. 3. Theoretical linkage of the Bennett mechanism in a parallel configuration.

By analogy, the screw $\boldsymbol{S}_6$ is

$$\boldsymbol{S}_6 = \left(0, \frac{\sqrt{2}}{2}, -\frac{\sqrt{2}}{2}, 0, -\frac{\sqrt{2}}{2}l, -\frac{\sqrt{2}}{2}l\right)^{\mathrm{T}} \tag{6}$$

Eqs. (5) and (6) give the angle δ as

$$\delta = \arccos\frac{1}{2}(-\cos\theta_1 - 1) \tag{7}$$

The coordinates of O' is

$$O' = \begin{bmatrix} \boldsymbol{R}_{x,-\alpha_{61}} & -a_{61}x \\ 0^{\mathrm{T}} & 1 \end{bmatrix} \begin{bmatrix} \boldsymbol{R}_{z,-\theta_6} & 0 \\ 0^{\mathrm{T}} & 1 \end{bmatrix} \begin{bmatrix} \boldsymbol{I} & -a_{46}x \\ 0^{\mathrm{T}} & 1 \end{bmatrix} \begin{pmatrix} 0 \\ 0 \\ 0 \\ 1 \end{pmatrix} \tag{8}$$

Substituting all the parameters of the Bennett mechanism into Eq. (8), we obtain

$$O' = \left(-l - l\cos\theta_6, -\frac{\sqrt{2}}{2}l\sin\theta_6, -\frac{\sqrt{2}}{2}l\sin\theta_6, 1\right)^{\mathrm{T}} \tag{9}$$

Hence, the distance from O to O' can be calculated as

$$\left|OO'\right| = \sqrt{2l(1+\cos\theta_6)} \tag{10}$$

This measures how close these two common parpendiculars are. When the result is zero, it indicates that two common parpendiculars coincide. Further, according to Baker [29], the relationship between θ_1 and θ_6 satisfies

$$\frac{\sqrt{2}}{2}\sin\frac{\theta_1}{2}\sin\frac{\theta_6}{2} + \cos\frac{\theta_1}{2}\cos\frac{\theta_6}{2} = 0 \tag{11}$$

When $\theta_1 = 0$, $\theta_6 = \pi$, the angle δ in Eq. (7) equals π that two axes of joints 3 and 6 are parallel and the distance $|OO'|$ in Eq. (10) equals 0, indicating two common perpendiculars coincide. Eq. (11) is also held. The Bennett mechanism comes to the parallel configuration shown in Fig. 3, where the axis of joint 3 is parallel with the axis of joint 6, the axes of joints 1 and 4 intersect at point O (O'). Fig. 4(a) uses bars to illustrate the Bennett mechanism in this configuration. When two new joints 2 and 5 are added to the Bennett mechanism, link L_{13} is replaced with L_{12} and L_{23}, link L_{46} is replaced with L_{45} and L_{56}, there will be a 6R metamorphic mechanism. There are two bases for adding these two joints. One is the line-symmetry constraint that provides a way of reconfigurability based on the screw system of the mechanism being able to transform from a screw system of the third order in line-symmetric to a screw system of the fifth order in line-symmetric. A further basis is that two conditions should be taken into consideration in order to generate both planar-motion branch and spherical-motion branch. These are parallel axes and intersecting axes, resulting in positions of new joints and lengths of new links.

In terms of the above two bases, new revolute joints 2 and 5 are added to the original Bennett mechanism as in Fig. 4(b). As the new 6R metamorphic mechanism needs to complete both planar and spherical motions, axes of joints 2 and 5 need to be parallel to axes of joints 3 and 6 and in intersecting axes of joints 1, and 4 at point O (O'). Thus, the positions of new joints and the lengths of new links are determined following these constraints. The positions of new joints and the lengths of new links are depicted by D-H parameters of the 6R metamorphic mechanism as

$$\begin{aligned} \alpha_{12} &= \alpha_{45} = \frac{\pi}{4},\ \alpha_{23} = \alpha_{56} = 0\ \alpha_{34} = \alpha_{61} = \frac{3\pi}{4} \\ a_{12} &= a_{45} = 0,\ a_{23} = a_{34} = a_{56} = a_{61} = l \\ d_1 &= d_2 = d_3 = d_4 = d_5 = d_6 = 0 \end{aligned} \tag{12}$$

where all the parameters are in Fig. 4(c). From the D-H parameters, it can be seen that the source mechanism is a special case of Bricard line-symmetric 6R mechanism [30,31].

Then the motion screws are

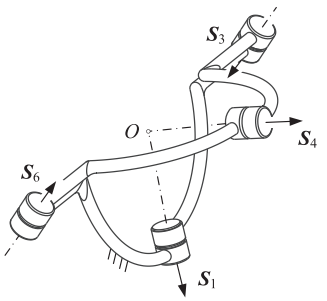

(a) Original equilateral Bennett mechanism in a parallel configuration

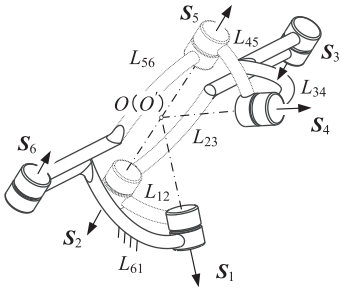

(b) new joints and links added to the original Bennett mechanism

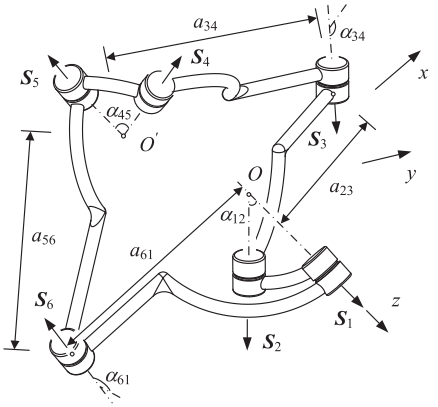

(c) parameters of the 6R metamorphic mechanism

Fig. 4. Parallel configuration of the Bennett mechanism, new added joints and parameters of the 6R metamorphic mechanism.

$$\boldsymbol{S}_1 = (0, 0, 1, 0, 0, 0)^{\mathrm{T}} \tag{13}$$

$$\boldsymbol{S}_2 = \left(\frac{\sqrt{2}}{2}\sin\theta_1, -\frac{\sqrt{2}}{2}\cos\theta_1, \frac{\sqrt{2}}{2}, 0, 0, 0\right)^{\mathrm{T}} \tag{14}$$

$$\boldsymbol{S}_3 = \left(\frac{\sqrt{2}}{2}\sin\theta_1, -\frac{\sqrt{2}}{2}\cos\theta_1, \frac{\sqrt{2}}{2}, l\cos\theta_1\sin\theta_2 + \frac{\sqrt{2}}{2}l\sin\theta_1\cos\theta_2, l\sin\theta_1\sin\theta_2 - \frac{\sqrt{2}}{2}l\cos\theta_1\cos\theta_2, -\frac{\sqrt{2}}{2}l\cos\theta_2\right)^{\mathrm{T}} \tag{15}$$

$$\begin{aligned}\boldsymbol{S}_4 = \Bigg(&\frac{\sqrt{2}}{2}\sin(\theta_5+\theta_6), -\frac{1}{2}\cos(\theta_5+\theta_6) + \frac{1}{2}, -\frac{1}{2}\cos(\theta_5+\theta_6) - \frac{1}{2}, \frac{\sqrt{2}}{2}l\sin\theta_6,\\ &-\frac{1}{2}l(\cos\theta_5+1)(\cos\theta_6+1) + \frac{1}{2}l\sin\theta_5\sin\theta_6, \frac{1}{2}l(\cos\theta_5-1)(\cos\theta_6+1) - \frac{1}{2}l\sin\theta_5\sin\theta_6\Bigg)^{\mathrm{T}}\end{aligned} \tag{16}$$

$$\boldsymbol{S}_5 = \left(0, \frac{\sqrt{2}}{2}, -\frac{\sqrt{2}}{2}, -l\sin\theta_6, -\frac{\sqrt{2}}{2}l - \frac{\sqrt{2}}{2}l\cos\theta_6, -\frac{\sqrt{2}}{2}l - \frac{\sqrt{2}}{2}l\cos\theta_6\right)^{\mathrm{T}} \tag{17}$$

$$\boldsymbol{S}_6 = \left(0, \frac{\sqrt{2}}{2}, -\frac{\sqrt{2}}{2}, 0, -\frac{\sqrt{2}}{2}l, -\frac{\sqrt{2}}{2}l\right)^{\mathrm{T}} \tag{18}$$

With the geometric relationship of the metamorphic mechanism, there will be different motion branches for the 6R metamorphic mechanism pending different motion trajectories. Each motion branch is decided by the relationship of joint angles. All screws form different geometry morphologies as discussed in the following sections.

3. The closure equation that lead to eight motion branches

For the 6R metamorphic mechanism, the global coordinate frame is set on L_{61} as in Fig. 4(c). z axis is along the axis of joint 1 and x axis is along the common normal of the axis of joint 6 and the axis of joint 1. Origin O is the intersection of x axis and z axis. y axis is decided by right-hand rule. The closure equation can be obtained as

$$\boldsymbol{H}_{12}\boldsymbol{H}_{23}\boldsymbol{H}_{34} = \boldsymbol{H}_{61}^{-1}\boldsymbol{H}_{56}^{-1}\boldsymbol{H}_{45}^{-1} \tag{19}$$

where

$$\boldsymbol{H}_{ij} = \begin{bmatrix} \cos\theta_i & -\sin\theta_i & 0 & 0 \\ \sin\theta_i & \cos\theta_i & 0 & 0 \\ 0 & 0 & 1 & d_i \\ 0 & 0 & 0 & 1 \end{bmatrix} \begin{bmatrix} 1 & 0 & 0 & a_{ij} \\ 0 & \cos\alpha_{ij} & -\sin\alpha_{ij} & 0 \\ 0 & \sin\alpha_{ij} & \cos\alpha_{ij} & 0 \\ 0 & 0 & 0 & 1 \end{bmatrix} \tag{20}$$

$$\boldsymbol{H}_{ij}^{-1} = \begin{bmatrix} 1 & 0 & 0 & -a_{ij} \\ 0 & \cos\alpha_{ij} & \sin\alpha_{ij} & 0 \\ 0 & -\sin\alpha_{ij} & \cos\alpha_{ij} & 0 \\ 0 & 0 & 0 & 1 \end{bmatrix} \begin{bmatrix} \cos\theta_i & \sin\theta_i & 0 & 0 \\ -\sin\theta_i & \cos\theta_i & 0 & 0 \\ 0 & 0 & 1 & -d_i \\ 0 & 0 & 0 & 1 \end{bmatrix} \tag{21}$$

in which a_{ij}, d_i, α_{ij} are the D-H parameters of the 6R metamorphic mechanism and θ_i is the angle of joint i.

Substituting all the D-H parameters of the 6R metamorphic mechanism in Eq. (12) into Eq. (19), we can obtain all the elements in the closure equation as listed in Appendix A. Adding the property of Bricard line-symmetric 6R mechanism [12], as

$$\begin{pmatrix}\theta_1 \\ \theta_2 \\ \theta_3\end{pmatrix} = \pm\begin{pmatrix}\theta_4 \\ \theta_5 \\ \theta_6\end{pmatrix} \tag{22}$$

that relates angular displacements θ_1, θ_2, θ_3 and θ_4, θ_5, θ_6, the closure equation in Appendix A and Eq. (22) determine the motion of the source mechanism and give two 6R configurations, three 4R configurations and further three configurations with two coaxial joints.

Rewriting Eqs. (A10), (A11) and (A12), we have

$$\begin{aligned} &l\cos\theta_1\cos\theta_2 + l\cos\theta_1(\cos\theta_2\cos\theta_3 - \sin\theta_2\sin\theta_3) \\ &\quad - \frac{\sqrt{2}}{2}l\sin\theta_1\sin\theta_2 - \frac{\sqrt{2}}{2}l\sin\theta_1(\sin\theta_2\cos\theta_3 + \cos\theta_2\sin\theta_3) \\ &= -l\cos\theta_6 - l \end{aligned} \tag{23}$$

$$\begin{aligned} &l\sin\theta_1\cos\theta_2 + l\sin\theta_1(\cos\theta_2\cos\theta_3 - \sin\theta_2\sin\theta_3) \\ &\quad + \frac{\sqrt{2}}{2}l\cos\theta_1\sin\theta_2 + \frac{\sqrt{2}}{2}l\cos\theta_1(\sin\theta_2\cos\theta_3 + \cos\theta_2\sin\theta_3) \\ &= -\frac{\sqrt{2}}{2}l\sin\theta_6 \end{aligned} \tag{24}$$

$$\frac{\sqrt{2}}{2}l\sin\theta_2 + \frac{\sqrt{2}}{2}l(\sin\theta_2\cos\theta_3 + \cos\theta_2\sin\theta_3) = -\frac{\sqrt{2}}{2}l\sin\theta_6 \tag{25}$$

Eliminating θ_6 in Eqs. (24) and (25), we obtain the constraint equation of the 6R metamorphic mechanism

$$l\sin\frac{\theta_1}{2}\cos\frac{\theta_3}{2}\left[\cos\frac{\theta_1}{2}\cos\left(\theta_2 + \frac{\theta_3}{2}\right) - \frac{\sqrt{2}}{2}\sin\frac{\theta_1}{2}\sin\left(\theta_2 + \frac{\theta_3}{2}\right)\right] = 0 \tag{26}$$

Meeting the condition of this geometric constraint equation in Eq. (26), following three equations exist. The first equation is

$$\cos\frac{\theta_1}{2}\cos\left(\theta_2 + \frac{\theta_3}{2}\right) - \frac{\sqrt{2}}{2}\sin\frac{\theta_1}{2}\sin\left(\theta_2 + \frac{\theta_3}{2}\right) = 0 \tag{27}$$

This gives a simplified version of the geometric constraint of the 6R metamorphic mechanism. Further, the constraint equation gives the following two alternatives

$$\sin\frac{\theta_1}{2}=0 \tag{28}$$

and

$$\cos\frac{\theta_3}{2}=0 \tag{29}$$

Three Eqs. (27) to (29) give three cases of geometric configurations for the 6R metamorphic mechanism. Eqs. (22) and (27) indicate no joints are geometrically constrained. Eqs. (22) and (28)indicate joints 1 and 4 are geometrically constrained at $\theta_1=\theta_4=0$. Eqs. (22) and (29) indicate joints 3 and 6 are geometrically constrained at $\theta_3=\theta_6=\pi$. Besides, when the sign in Eq. (22) is (−), through Eq. (25), a further case of geometric configurations for the 6R metamorphic mechanism can be obtained as

$$l\sin\frac{\theta_2}{2}\cos\frac{\theta_3}{2}\cos\frac{\theta_2+\theta_3}{2}=0 \tag{30}$$

One solution of Eq. (30) is

$$\sin\frac{\theta_2}{2}=0 \tag{31}$$

Eq. (31) gives the fourth condition with joints 2 and 5 geometrically constrained at $\theta_2=\theta_5=0$.

Thus, there are two conditions for joints i and $i+3$ ($i=1, 2, 3$). They can be moveable or be geometrically constrained. When Eq. (27) is held, all joints are geometrically unconstrained and the 6R metamorphic mechanism runs into two 6R motion branches. When only one of Eqs. (28), (29) and (31) is held, that is, one group of joints i and $i+3$ is geometrically constrained, there remain only four joints being geometrically unconstained. Thus the metamorphic mechanism runs into 4R motion branches. Besides, when two groups of joints i and $i+3$ are geometrically constrained, the joints will be coaxial. The metamorphic mechanism runs into the motion branches with two coaxial joints. All motion branches will be analyzed as follows.

3.1. Two 6R motion branches—bricard motion branches (BB_1, BB_2)

When Eq. (27) is held, all joints are geometrically unconstrained. This results in the 6R motion branches of the metamorphic mechanism.

When the sign in Eq. (22) is (+) (the condition that the sign in Eq. (22) is (−) will be discussed later, and the two different conditions are all taken into consideration under all motion branches), Eq. (25) gives

$$\sin\frac{\theta_2+\theta_3}{2}=0 \tag{32}$$

then

$$\frac{1}{2}\sin\theta_1\cos(\theta_2+\theta_3)=\frac{1}{2}\sin\theta_1 \tag{33}$$

Adding Eq. (33) at both sides of Eq. (A7), we have

$$\left(-\frac{\sqrt{2}}{2}\sin\frac{\theta_1}{2}\sin\theta_3+\cos\frac{\theta_1}{2}\cos\theta_3\right)\cos\theta_2+\left(-\frac{\sqrt{2}}{2}\sin\frac{\theta_1}{2}\cos\theta_3-\cos\frac{\theta_1}{2}\sin\theta_3\right)\sin\theta_2=\cos\frac{\theta_1}{2} \tag{34}$$

which is the same as the result in Baker [32].

Rewriting Eq. (23), we have

$$\left(\cos\theta_1\cos\frac{\theta_3}{2}-\frac{\sqrt{2}}{2}\sin\theta_1\sin\frac{\theta_3}{2}\right)\cos\theta_2+\left(-\frac{\sqrt{2}}{2}\sin\theta_1\cos\frac{\theta_3}{2}-\cos\theta_1\sin\frac{\theta_3}{2}\right)\sin\theta_2=-\cos\frac{\theta_3}{2} \tag{35}$$

Eliminating θ_2 in Eqs. (34) and (35), we obtain

$$\left[\sin^3\frac{\theta_1}{2}\cos\frac{\theta_1}{2}\sin\frac{\theta_3}{2}+\sqrt{2}\left(1+\cos^4\frac{\theta_1}{2}\right)\cos\frac{\theta_3}{2}\right]$$
$$\cos\frac{\theta_1}{2}\left(\sqrt{2}\cos\frac{\theta_1}{2}\cos\frac{\theta_3}{2}+\sin\frac{\theta_1}{2}\sin\frac{\theta_3}{2}\right)=0 \tag{36}$$

which gives two motion branches with all joints being geometrically unconstrained. One is given by the solution of Eq. (36) as

$$\sqrt{2}\cos\frac{\theta_1}{2}\cos\frac{\theta_3}{2}+\sin\frac{\theta_1}{2}\sin\frac{\theta_3}{2}=0 \tag{37}$$

that gives the first 6R motion branch. The other solution of Eq. (36) is

$$\sin^3\frac{\theta_1}{2}\cos\frac{\theta_1}{2}\sin\frac{\theta_3}{2}+\sqrt{2}\left(1+\cos^4\frac{\theta_1}{2}\right)\cos\frac{\theta_3}{2}=0 \tag{38}$$

which gives the second 6R motion branch.

When the sign in Eq. (22) is (−), Eq. (25) gives

$$\cos\frac{\theta_2+\theta_3}{2}=0 \tag{39}$$

Eqs. (39) and (A7) result in a geometric constraint that $\theta_1=\theta_4=0$ or $\theta_1=\theta_4=\pi$. Thus, the metamorphic mechanism transforms from a 6R motion branch to a 4R motion branch that is excluded in this discussion in Section 3a and will be analyzed in the following section.

Therefore, there are only two 6R motion branches for the 6R metamorphic mechanism. Both motion branches are Bricard line-symmetric 6R motion branches.

3.2. Three 4R motion branches—planar motion branch (PB), spherical motion branch (SB), bennett motion branch (NB)

When Eq. (28) is held and neither of Eqs. (29) and (31) is satisfied, $\theta_1=\theta_4=0$ and joints 2, 3, 5, 6 are geometrically unconstrained. Eliminating θ_6 in Eqs. (23) and (25), we have

$$\cos\frac{\theta_2+\theta_3}{2}\cos\frac{\theta_2}{2}\cos\frac{\theta_3}{2}=0 \tag{40}$$

As joints 2 and 3 are not geometrically constrained, Eq. (39) is the solution of Eq. (40), which gives $\theta_2+\theta_3=\pm\pi$. Using Eq. (25), it derives $\theta_3=-\theta_6$ and $\theta_2=-\theta_5$. Then the sign in Eq. (22) is (−). That gives the first 4R motion branch.

When Eq. (29) is held and neither of Eqs. (28) and (31) is satisfied, $\theta_3=\theta_6=\pi$ and joints 1, 2, 4, 5 are geometrically unconstrained. Simplifying Eq. (A8), it derives

$$\sin\frac{\theta_1}{2}\cos\frac{\theta_2}{2}\left(\frac{\sqrt{2}}{2}\sin\frac{\theta_2}{2}\cos\frac{\theta_1}{2}+\frac{1}{2}\sin\frac{\theta_1}{2}\cos\frac{\theta_2}{2}\right)=0 \tag{41}$$

this gives

$$\frac{\sqrt{2}}{2}\sin\frac{\theta_2}{2}\cos\frac{\theta_1}{2}+\frac{1}{2}\sin\frac{\theta_1}{2}\cos\frac{\theta_2}{2}=0 \tag{42}$$

Further, Eq. (A7) becomes

$$-\frac{\sqrt{2}}{2}\cos\theta_1\sin\theta_2+\frac{\sqrt{2}}{2}\sin\theta_5-\frac{1}{2}\sin\theta_1(\cos\theta_2+1)=0 \tag{43}$$

When the sign in Eq. (22) is (+), Eq. (43) becomes

$$\sin\frac{\theta_1}{2}\cos\frac{\theta_2}{2}\left(\frac{\sqrt{2}}{2}\sin\frac{\theta_2}{2}\sin\frac{\theta_1}{2}+\frac{1}{2}\cos\frac{\theta_1}{2}\cos\frac{\theta_2}{2}\right)=0 \tag{44}$$

Eqs. (42) and (44) cannot be held at the same time, which indicates the sign in Eq. (22) is (−). That gives the second 4R motion branch.

When Eq. (31) is held and neither of Eqs. (28) and (29) is satisfied, $\theta_2=\theta_5=0$ and joints that are geometricaly unconstrained are joints 1, 3, 4, 6. Simplifying Eq. (23), it derives

$$\cos\frac{\theta_1}{2}\cos\frac{\theta_3}{2}\left(\cos\frac{\theta_1}{2}\cos\frac{\theta_3}{2}-\frac{\sqrt{2}}{2}\sin\frac{\theta_1}{2}\sin\frac{\theta_3}{2}\right)=0 \tag{45}$$

which gives

$$\cos\frac{\theta_1}{2}\cos\frac{\theta_3}{2}-\frac{\sqrt{2}}{2}\sin\frac{\theta_1}{2}\sin\frac{\theta_3}{2}=0 \tag{46}$$

From Eq. (30), we obtain the sign in Eq. (22) is (−). That gives the third 4R motion branch.

As discussed above, when only one group of joints i and $i+3$ are geometrically constrained, there are three 4R motion branches which are revealed as a planar-motion branch, a spherical-motion branch and a Bennett-motion branch.

3.3. Three motion branches with coaxial joints—coaxial branches (CB_1, CB_2, CB_3)

Further, when two groups of joints i and $i+3$ are geometrically constrained, the joints in the left will be coaxial. The 6R metamorphic mechanism will go to the motion branches with two coaxial joints.

Table 1
Geometric constraint of the eight motion branches of the 6R metamorphic mechanism.

Case	Type	Sign in Eq. (22)	Geometric constraint
I	Bricard line-symmetric 6R motion branch (BB_1)	+	$\sin\frac{\theta_2+\theta_3}{2}=0$ Eq. (32) $\sqrt{2}\cos\frac{\theta_1}{2}\cos\frac{\theta_3}{2}+\sin\frac{\theta_1}{2}\sin\frac{\theta_3}{2}=0$ Eq. (37)
II	Bricard line-symmetric 6R motion branch (BB_1)	+	$\sin\frac{\theta_2+\theta_3}{2}=0$ Eq. (32) $\sin^3\frac{\theta_1}{2}\cos\frac{\theta_1}{2}\sin\frac{\theta_3}{2}+\sqrt{2}(1+\cos^4\frac{\theta_1}{2})\cos\frac{\theta_3}{2}=0$ Eq. (38)
III	Planar 4R motion branch (PB)	−	$sin\frac{\theta_1}{2}=0$ Eq. (28) $\cos\frac{\theta_2+\theta_3}{2}=0$ Eq. (39)
IV	Spherical 4R motion branch (SB)	−	$\cos\frac{\theta_3}{2}=0$ Eq. (29) $\frac{\sqrt{2}}{2}\sin\frac{\theta_2}{2}\cos\frac{\theta_1}{2}+\frac{1}{2}\sin\frac{\theta_1}{2}\cos\frac{\theta_2}{2}=0$ Eq. (42)
V	Bennett-motion branch (NB)	−	$\sin\frac{\theta_2}{2}=0$ Eq. (31) $\cos\frac{\theta_1}{2}\cos\frac{\theta_3}{2}-\frac{\sqrt{2}}{2}\sin\frac{\theta_1}{2}\sin\frac{\theta_3}{2}=0$ Eq. (46)
VI	Motion branch with joints 2 and 5 being coaxial (CB_1)	+	$sin\frac{\theta_1}{2}=0$ Eq. (28) $\sin\theta_2=\sin\theta_5$ Eq. (47)
VII	Motion branch with joints 3 and 6 being coaxial (CB_2)	+	$sin\frac{\theta_1}{2}=0$ Eq. (28) $\sin\theta_3=\sin\theta_6$ Eq. (48)
VIII	Motion branch with joints 1 and 4 being coaxial (CB_3)	+	$\cos\frac{\theta_3}{2}=0$ Eq. (29) $\sin\theta_1=\sin\theta_4$ Eq. (49)

One solution of Eq. (40) is $\cos\frac{\theta_3}{2}=0$. This indicates joints 2 and 5 will be coaxial. Eq. (A7) gives

$$\sin\theta_2=\sin\theta_5 \tag{47}$$

which means the sign in Eq. (22) is (+).

Another solution of Eq. (40) is $\cos\frac{\theta_2}{2}=0$. This indicates joints 3 and 6 are coaxial. Eq. (A7) gives

$$\sin\theta_3=\sin\theta_6 \tag{48}$$

which means the sign in Eq. (22) is (+).

Besides, one solution to Eq. (41) is $\cos\frac{\theta_2}{2}=0$. This indicates joints 1 and 4 are coaxial.

$$\sin\theta_1=\sin\theta_4 \tag{49}$$

which means the sign in Eq. (22) is (+).

Therefore, the three motion branches with coaxial joints of the 6R metamorphic mechanism are given.

From the above, there are totally eight motion branches of the novel 6R metamorphic mechanism. Table 1 defines all the motion branches and the corresponding geometric constraint. The corresponding geometry morphology of each motion branch will be analyzed using screw theory in next section.

4. Corresponding geometry morphologies of different mechanism configurations of eight motion branches

4.1. Mechanism configurations of two 6R motion branches

For the first 6R motion branch, the screws become

$$\boldsymbol{S}_1=(0,0,1,0,0,0)^{\mathrm{T}} \tag{50}$$

$$\boldsymbol{S}_2=\left(\frac{\sqrt{2}}{2}\sin\theta_1,-\frac{\sqrt{2}}{2}\cos\theta_1,\frac{\sqrt{2}}{2},0,0,0\right)^{\mathrm{T}} \tag{51}$$

$$\boldsymbol{S}_3=\left(\frac{\sqrt{2}}{2}\sin\theta_1,-\frac{\sqrt{2}}{2}\cos\theta_1,\frac{\sqrt{2}}{2},l\cos\theta_1\sin\theta_2+\frac{\sqrt{2}}{2}l\sin\theta_1\cos\theta_2,l\sin\theta_1\sin\theta_2-\frac{\sqrt{2}}{2}l\cos\theta_1\cos\theta_2,-\frac{\sqrt{2}}{2}l\cos\theta_2\right)^{\mathrm{T}} \tag{52}$$

$$\boldsymbol{S}_4=\left(0,0,-1,\frac{\sqrt{2}}{2}l\sin\theta_6,-\frac{1}{2}l(\cos\theta_5+1)(\cos\theta_6+1)+\frac{1}{2}l\sin\theta_5\sin\theta_6,\frac{1}{2}l(\cos\theta_5-1)(\cos\theta_6+1)-\frac{1}{2}l\sin\theta_5\sin\theta_6\right)^{\mathrm{T}} \tag{53}$$

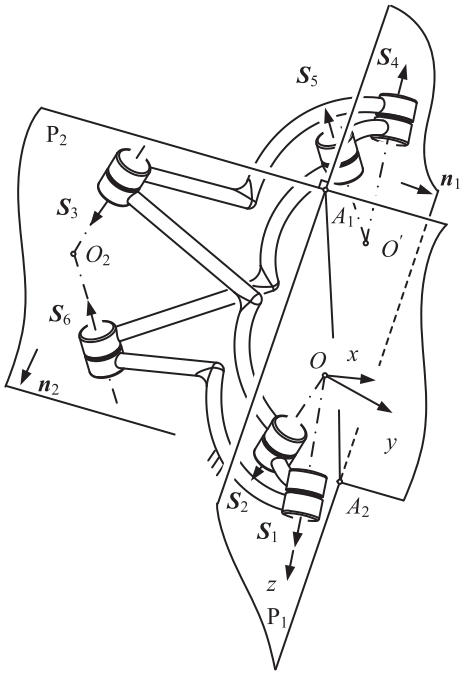

Fig. 5. One configuration of the first Bricard line-symmetric 6R motion branch.

$$\boldsymbol{S}_5 = \left(0, \frac{\sqrt{2}}{2}, -\frac{\sqrt{2}}{2}, -l\sin\theta_6, -\frac{\sqrt{2}}{2}l - \frac{\sqrt{2}}{2}l\cos\theta_6, -\frac{\sqrt{2}}{2}l - \frac{\sqrt{2}}{2}l\cos\theta_6\right)^{\mathrm{T}} \tag{54}$$

$$\boldsymbol{S}_6 = \left(0, \frac{\sqrt{2}}{2}, -\frac{\sqrt{2}}{2}, 0, -\frac{\sqrt{2}}{2}l, -\frac{\sqrt{2}}{2}l\right)^{\mathrm{T}} \tag{55}$$

Using the reciprocal product of two screws in Ref. [33], we obtain

$$\boldsymbol{S}_3 \circ \boldsymbol{S}_6 = \left[\frac{\sqrt{2}}{2}\sin\theta_1\sin\theta_2 - \frac{1}{2}(1-\cos\theta_1)(1-\cos\theta_2)\right]l \tag{56}$$

From Eqs. (32) and (37), it can be derived that the reciprocal product of $\boldsymbol{S}_3$ and $\boldsymbol{S}_6$ is zero. This results in joint 3 intersects joint 6. Further, Eqs. (50) and (53) indicate $\boldsymbol{S}_1$ and $\boldsymbol{S}_4$ are parallel.

One configuration of the 6R motion branch is shown in Fig. 5. $\boldsymbol{S}_3$ intersects $\boldsymbol{S}_6$ at O_2. There are a plane P_1 passing through joint $\boldsymbol{S}_1$ and $\boldsymbol{S}_4$, and a plane P_2 passing through $\boldsymbol{S}_3$ and $\boldsymbol{S}_6$. P_1 intersects P_2 at line A_1A_2.

Using the coordinates of the point O' $(-l\cos\theta_6 - l, -\frac{\sqrt{2}}{2}l\sin\theta_6, -\frac{\sqrt{2}}{2}l\sin\theta_6, 1)^{\mathrm{T}}$ on $\boldsymbol{S}_4$, the direction of $\boldsymbol{S}_1$ and the origin O $(0, 0, 0, 1)^{\mathrm{T}}$ on $\boldsymbol{S}_1$, we obtain the normal vector of P_1

$$\boldsymbol{n}_1 = \left(\frac{\sqrt{2}}{2}\sin\theta_6, -\cos\theta_6 - 1, 0\right)^{\mathrm{T}} \tag{57}$$

Using the direction vectors of $\boldsymbol{S}_3$ and $\boldsymbol{S}_6$, the normal vector of P_2 is

$$\boldsymbol{n}_2 = \left(\frac{1}{2}\cos\theta_1 - \frac{1}{2}, \frac{1}{2}\sin\theta_1, \frac{1}{2}\sin\theta_1\right)^{\mathrm{T}} \tag{58}$$

then the scalar product of $\boldsymbol{n}_1$ and $\boldsymbol{n}_2$ is

$$\boldsymbol{n}_1 \cdot \boldsymbol{n}_2 = \frac{\sqrt{2}}{4}\sin\theta_6(\cos\theta_1 - 1) - \frac{1}{2}\sin\theta_1(\cos\theta_6 + 1) \tag{59}$$

From Eqs. (22) and (37), it can be derived that $\boldsymbol{n}_1 \cdot \boldsymbol{n}_2 = 0$, which indicates P_1 is perpendicular to P_2 at A_1A_2. This is the geometry morphology of all the joints for the first Bricard line-symmetric motion branch.

For the second 6R motion branch, the screws remain the same with the first one. Thus, $\boldsymbol{S}_1$ and $\boldsymbol{S}_4$ are still parallel. Fig. 6 shows one configuration of this 6R motion branch. There is a plane P passing through $\boldsymbol{S}_1$ and $\boldsymbol{S}_4$. This is the geometry morphology of all the joints for the second Bricard line-symmetric motion branch.

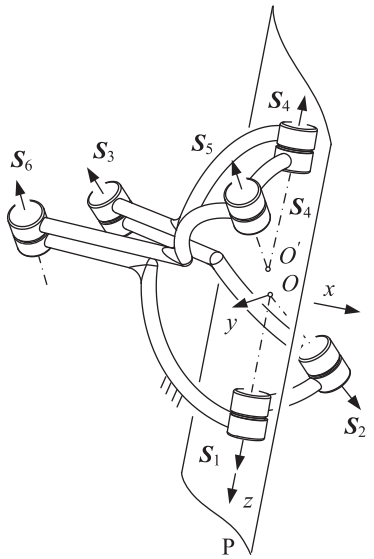

Fig. 6. One configuration of the second Bricard line-symmetric 6R motion branch.

Notice that, all the joints of the motion branch in Fig. 5 have a full revolution while only joints 1 and 4 of the motion branch in Fig. 6 have a full revolution.

4.2. Mechanism configurations of three 4R motion branches

For the first 4R motion branch, it is of a planar 4R mechanism configuration. The screws become

$$\boldsymbol{S}_1 = (0, 0, 1, 0, 0, 0)^{\mathrm{T}} \tag{60}$$

$$\boldsymbol{S}_2 = \left(0, -\frac{\sqrt{2}}{2}, \frac{\sqrt{2}}{2}, 0, 0, 0\right)^{\mathrm{T}} \tag{61}$$

$$\boldsymbol{S}_3 = \left(0, -\frac{\sqrt{2}}{2}, \frac{\sqrt{2}}{2}, l\sin\theta_2, -\frac{\sqrt{2}}{2}l\cos\theta_2, -\frac{\sqrt{2}}{2}l\cos\theta_2\right)^{\mathrm{T}} \tag{62}$$

$$\boldsymbol{S}_4 = \left(0, 1, 0, -\frac{\sqrt{2}}{2}l\sin\theta_3, 0, -l + l\cos\theta_2\right)^{\mathrm{T}} \tag{63}$$

$$\boldsymbol{S}_5 = \left(0, \frac{\sqrt{2}}{2}, -\frac{\sqrt{2}}{2}, l\sin\theta_3, -\frac{\sqrt{2}}{2}l + \frac{\sqrt{2}}{2}l\cos\theta_3, -\frac{\sqrt{2}}{2}l + \frac{\sqrt{2}}{2}l\cos\theta_3\right)^{\mathrm{T}} \tag{64}$$

$$\boldsymbol{S}_6 = \left(0, \frac{\sqrt{2}}{2}, -\frac{\sqrt{2}}{2}, 0, -\frac{\sqrt{2}}{2}l, -\frac{\sqrt{2}}{2}l\right)^{\mathrm{T}} \tag{65}$$

It is noted that, because joints 1 and 4 are geometrically constrained, the four geometrically unconstrained joints are 2, 3, 5 and 6. From the screws, we obtain that $\boldsymbol{S}_2$, $\boldsymbol{S}_3$, $\boldsymbol{S}_5$ and $\boldsymbol{S}_6$ are parallel. The four geometrically unconstrained joints form a planar-motion branch as in Fig. 7. There are one plane P_3 passing through $\boldsymbol{S}_3$, $\boldsymbol{S}_6$ and another plane P_4 passing through $\boldsymbol{S}_2$, $\boldsymbol{S}_5$. The intersection of the two planes is line A_3A_4.

Using the point B_1 $(-l, 0, 0, 1)^{\mathrm{T}}$on $\boldsymbol{S}_6$, the point B_2 $(l\cos\theta_2, \frac{\sqrt{2}}{2}l\sin\theta_2, \frac{\sqrt{2}}{2}l\sin\theta_2, 1)^{\mathrm{T}}$ on $\boldsymbol{S}_3$, and the direction of $\boldsymbol{S}_6$, we obtain the normal vector of P_3

$$\boldsymbol{n}_3 = \left(\sqrt{2}\sin\theta_2, -1 - \cos\theta_2, -1 - \cos\theta_2\right)^{\mathrm{T}} \tag{66}$$

Further, the normal vector of P_4 is

$$\boldsymbol{n}_4 = \left(\sqrt{2}\sin\theta_2, 1 - \cos\theta_2, 1 - \cos\theta_2\right)^{\mathrm{T}} \tag{67}$$

Then $\boldsymbol{n}_3 \cdot \boldsymbol{n}_4 = 0$. The scalar product of the two normal vectors equals zero and this indicates P_3 is perpendicular to P_4 at A_3A_4. This is the geometry morphology of the four geometrically unconstrained joints for the planar-motion branch.

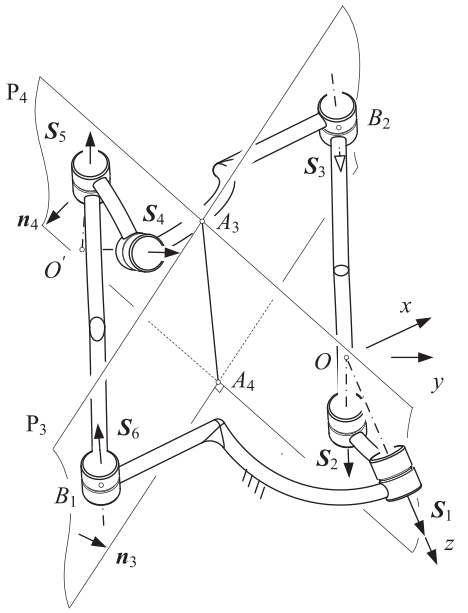

Fig. 7. One configuration of the planar-motion branch.

For the second 4R motion branch, it is of a spherical 4R mechanism configuration. Thus, the screws become

$$\boldsymbol{S}_1 = (0, 0, 1, 0, 0, 0)^{\mathrm{T}} \tag{68}$$

$$\boldsymbol{S}_2 = \left(\frac{\sqrt{2}}{2}\sin\theta_1, -\frac{\sqrt{2}}{2}\cos\theta_1, \frac{\sqrt{2}}{2}, 0, 0, 0 \right)^{\mathrm{T}} \tag{69}$$

$$\begin{aligned} \boldsymbol{S}_3 = \Big(& \tfrac{\sqrt{2}}{2}\sin\theta_1, -\tfrac{\sqrt{2}}{2}\cos\theta_1, \tfrac{\sqrt{2}}{2}, l\cos\theta_1\sin\theta_2 + \tfrac{\sqrt{2}}{2}l\sin\theta_1\cos\theta_2, \\ & l\sin\theta_1\sin\theta_2 - \tfrac{\sqrt{2}}{2}l\cos\theta_1\cos\theta_2, -\tfrac{\sqrt{2}}{2}l\cos\theta_2 \Big)^{\mathrm{T}} \end{aligned} \tag{70}$$

$$\boldsymbol{S}_4 = \left(-\frac{\sqrt{2}}{2}\sin\theta_5, \frac{1}{2}\cos\theta_5 + \frac{1}{2}, \frac{1}{2}\cos\theta_5 - \frac{1}{2}, 0, 0, 0 \right)^{\mathrm{T}} \tag{71}$$

$$\boldsymbol{S}_5 = \left(0, \frac{\sqrt{2}}{2}, -\frac{\sqrt{2}}{2}, 0, 0, 0 \right)^{\mathrm{T}} \tag{72}$$

$$\boldsymbol{S}_6 = \left(0, \frac{\sqrt{2}}{2}, -\frac{\sqrt{2}}{2}, 0, -\frac{\sqrt{2}}{2}l, -\frac{\sqrt{2}}{2}l \right)^{\mathrm{T}} \tag{73}$$

Because joints 3 and 6 are geometrically constrained, the four geometrically unconstrained joints are joints 1, 2, 4 and 5. From the screws, it can be obtained that $\boldsymbol{S}_1$, $\boldsymbol{S}_2$, $\boldsymbol{S}_4$ and $\boldsymbol{S}_5$ are concurrent at point O. The four geometrically unconstrained joints form a spherical-motion branch as in Fig. 8. There are a plane P_5 passing through $\boldsymbol{S}_2$ and $\boldsymbol{S}_5$, and another plane P_6 passing through $\boldsymbol{S}_1$ and $\boldsymbol{S}_4$. The intersection of the two planes is line A_5A_6 and O is on A_5A_6. Using the direction vectors of $\boldsymbol{S}_2$, $\boldsymbol{S}_5$ in Eqs. (69) and (72), we obtain the normal vector of P_5

$$\boldsymbol{n}_5 = \left(-\frac{1}{2}\cos\theta_1 + \frac{1}{2}, -\frac{1}{2}\sin\theta_1, -\frac{1}{2}\sin\theta_1 \right)^{\mathrm{T}} \tag{74}$$

Using the direction vectors of $\boldsymbol{S}_1$, $\boldsymbol{S}_4$ in Eqs. (68) and (71), we obtain the normal vector of P_6

$$\boldsymbol{n}_6 = \left(-\frac{1}{2}\cos\theta_5 - \frac{1}{2}, -\frac{\sqrt{2}}{2}\sin\theta_5, 0 \right)^{\mathrm{T}} \tag{75}$$

then we have

$$\boldsymbol{n}_5 \cdot \boldsymbol{n}_6 = \frac{\sqrt{2}}{2}\sin\theta_1\sin\theta_5 + \frac{1}{2}(\cos\theta_1 - 1)(\cos\theta_5 + 1) \tag{76}$$

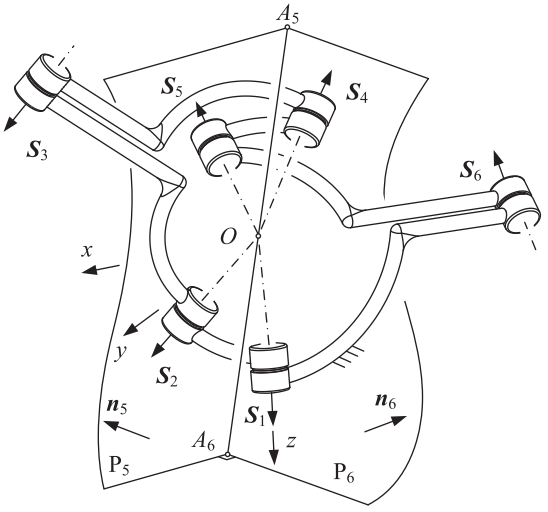

Fig. 8. One configuration of the spherical-motion branch.

From Eqs. (22), (42), (74) and (75), it can be derived that $\boldsymbol{n}_5 \cdot \boldsymbol{n}_6 = 0$, which indicates P_5 is perpendicular to P_6 at A_5A_6. This is the geometry morphology of the four geometrically unconstrained joints for spherical-motion branch.

For the third 4R motion branch, it is of a Bennett mechanism configuration. Thus, the screws become

$$\boldsymbol{S}_1 = (0, 0, 1, 0, 0, 0)^{\mathrm{T}} \tag{77}$$

$$\boldsymbol{S}_2 = \left(\frac{\sqrt{2}}{2}\sin\theta_1, -\frac{\sqrt{2}}{2}\cos\theta_1, \frac{\sqrt{2}}{2}, 0, 0, 0\right)^{\mathrm{T}} \tag{78}$$

$$\boldsymbol{S}_3 = \left(\frac{\sqrt{2}}{2}\sin\theta_1, -\frac{\sqrt{2}}{2}\cos\theta_1, \frac{\sqrt{2}}{2}, \frac{\sqrt{2}}{2}l\sin\theta_1, -\frac{\sqrt{2}}{2}l\cos\theta_1, -\frac{\sqrt{2}}{2}l\right)^{\mathrm{T}} \tag{79}$$

$$\boldsymbol{S}_4 = \left(\frac{\sqrt{2}}{2}\sin\theta_6, -\frac{1}{2}\cos\theta_6 + \frac{1}{2}, -\frac{1}{2}\cos\theta_6 - \frac{1}{2}, \frac{\sqrt{2}}{2}l\sin\theta_6, -l(\cos\theta_6 + 1), 0\right)^{\mathrm{T}} \tag{80}$$

$$\boldsymbol{S}_5 = \left(0, \frac{\sqrt{2}}{2}, -\frac{\sqrt{2}}{2}, -l\sin\theta_6, -\frac{\sqrt{2}}{2}l - \frac{\sqrt{2}}{2}l\cos\theta_6, -\frac{\sqrt{2}}{2}l - \frac{\sqrt{2}}{2}l\cos\theta_6\right)^{\mathrm{T}} \tag{81}$$

$$\boldsymbol{S}_6 = \left(0, \frac{\sqrt{2}}{2}, -\frac{\sqrt{2}}{2}, 0, -\frac{\sqrt{2}}{2}l, -\frac{\sqrt{2}}{2}l\right)^{\mathrm{T}} \tag{82}$$

It is noted that, because joints 2 and 5 are geometrically constrained, the four geometrically unconstrained joints are 1, 3, 4 and 6. Thus, $\boldsymbol{S}_1$ intersects $\boldsymbol{S}_4$ at O_1 and $\boldsymbol{S}_3$ intersects $\boldsymbol{S}_6$ at point O_2. The four geometrically unconstrained joints form a Bennett-motion branch as in Fig. 9. There are a plane P_7 passing through $\boldsymbol{S}_1$ and $\boldsymbol{S}_4$, and another plane P_8 passing through $\boldsymbol{S}_3$ and $\boldsymbol{S}_6$. The intersection of the two planes is line O_1O_2. Using the direction vectors of $\boldsymbol{S}_1$, $\boldsymbol{S}_4$, we obtain the normal vector of P_7

$$\boldsymbol{n}_7 = \left(\frac{1}{2}\cos\theta_6 - \frac{1}{2}, \frac{\sqrt{2}}{2}\sin\theta_6, 0\right)^{\mathrm{T}} \tag{83}$$

Further, from the direction vectors of $\boldsymbol{S}_3$, $\boldsymbol{S}_6$, we obtain the normal vector of P_8

$$\boldsymbol{n}_8 = \left(\frac{1}{2}\cos\theta_1 - \frac{1}{2}, \frac{1}{2}\sin\theta_1, \frac{1}{2}\sin\theta_1\right)^{\mathrm{T}} \tag{84}$$

From Eqs. (22), (45), (83) and (84), it can be derived that $\boldsymbol{n}_7 \cdot \boldsymbol{n}_8 = 0$, which indicates P_7 is perpendicular to P_8 at O_1O_2. This is the geometry morphology of the four geometrically unconstrained joints for Bennett-motion branch.

It is noticed that the geometrically unconstrained joints in each of 4R motion branch are corresponding to a geometry morphology of screw system of the third order [33].

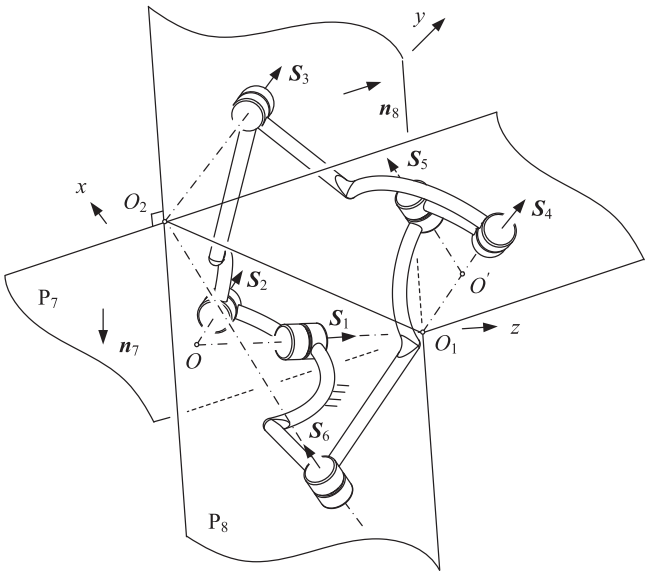

Fig. 9. One configuration of Bennett-motion branch.

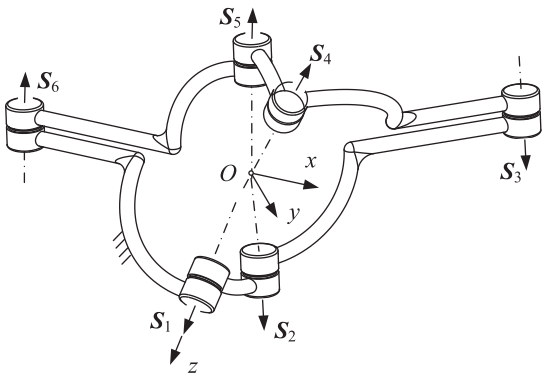

Fig. 10. One configuration of the motion branch when joints 2 and 5 are coaxial.

4.3. Three motion branches with coaxial joints

As mentioned above, the 6R metamorphic mechanism has three motion branches with two coaxial joints. When joints 2 and 5 are coaxial, the motion branch is shown in Fig. 10.

When joints 3 and 6 are coaxial, the motion branch is shown in Fig. 11.

When joints 1 and 4 are coaxial, the motion branch is shown in Fig. 12.

5. Furcation points and metamorphosis between motion branches

As discussed above, there are eight motion branches for the 6R metamorphic mechanism. The first Bricard motion branch in Fig. 5 is marked as BB_1, and the second Bricard motion branch in Fig. 6 is marked as BB_2. BB_1 and BB_2 are the two 6R motion branches. The planar-motion branch in Fig. 7 is marked as *PB*, the spherical-motion branch in Fig. 8 is marked as *SB*, and the Bennett-motion branch in Fig. 9 is marked as *NB*. *PB, SB* and *NB* are the three 4R motion branches. The motion branch with joints 2 and 5 coaxial in Fig. 10 is marked as CB_1, the motion branch with joints 3 and 6 coaxial in Fig. 11 is marked as CB_2, the motion branch with joints 1 and 4 coaxial in Fig. 12 is marked as CB_3. CB_1, CB_2 and CB_3 are the motion branches with two coaxial joints.

Based on geometric constraint equations of different motion branches, two bifurcation points, one trifurcation point and two multi-furcation points are figured out as follows.

$\theta_1 = -\pi$, $\theta_2 = 2\pi$ and $\theta_3 = 0$ are the solution to Eqs. (31), (32), (37) and (46), which satisfies the relationship of the joints for the first Bricard motion branch BB_1 and the Bennett-motion branch *NB*. Therefore, it is a bifurcation point of the 6R metamorphic mechanism. We mark the joint angles θ_1, θ_2, θ_3 here as bifurcation point B_1.

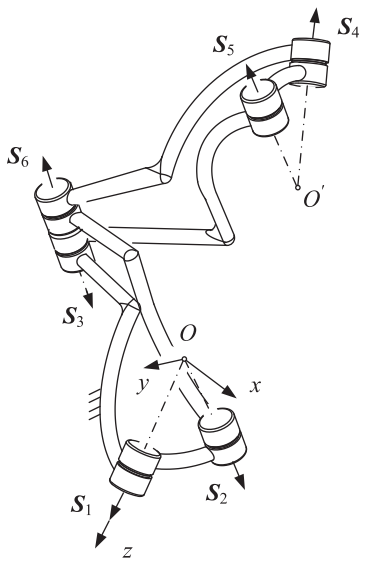

Fig. 11. One configuration of the motion branch when joints 3 and 6 are coaxial.

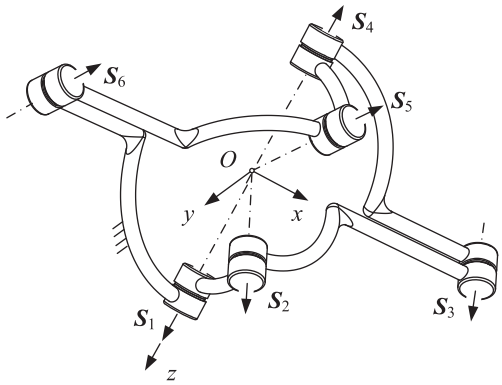

Fig. 12. One configuration of the motion branch when joints 1 and 4 are coaxial.

$\theta_1 = 0$, $\theta_2 = \pi$ and $\theta_3 = 2\pi$ are the solution to Eqs. (28), (39) and (48), which satisfies the relationship of the joints for motion branches the planar-motion branch *PB* and the motion branch with joints 3 and 6 coaxial CB_2. Therefore, it is another bifurcation point of the 6R metamorphic mechanism. We mark the joint angles θ_1, θ_2, θ_3 here as bifurcation point B_2.

$\theta_1 = -\pi$, $\theta_2 = \pi$ and $\theta_3 = \pi$ are the solution to Eqs. (29), (32), (38), (42) and (49), which satisfies the relationship of the joints for motion branches the second Bricard motion branch BB_2, the spherical-motion branch *SB* and the motion branch with joints 1 and 4 coaxial CB_3. Therefore, it is a trifurcation point of the 6R metamorphic mechanism. We mark the joint angles θ_1, θ_2, θ_3 as trifurcation point T_1.

$\theta_1 = 0$, $\theta_2 = 2\pi$ and $\theta_3 = \pi$ are the solution to Eqs. (28), (29), (31), (39), (42), (46) and (48), which satisfies the relationship of the joints for motion branches the planar-motion branch *PB*, the spherical-motion branch *SB*, the Bennett-motion branch *NB* and the motion branch with joints 2 and 5 coaxial CB_1. Therefore, it is a multi-furcation point of the 6R metamorphic mechanism. We mark the joint angles θ_1, θ_2, θ_3 as multi-furcation point F_1.

$\theta_1 = 0$, $\theta_2 = \pi$ and $\theta_3 = \pi$ are the solution to Eqs. (28), (29), (32), (37), (38), (47), (48) and (49), which satisfies the relationship of the joints for the first Bricard motion branch BB_1, the second Bricard motion branch BB_2, the motion branch with joints 2 and 5 coaxial CB_1, the motion branch with joints 3 and 6 coaxial CB_2 and the motion branch with joints 1 and 4 coaxial CB_3. Therefore, it is another multi-furcation point of the 6R metamorphic mechanism. We mark the joint angles θ_1, θ_2, θ_3 as multi-furcation point F_2.

As the novel 6R metamorphic mechanism is a special and extended part of the Bricard line-symmetric mechanism, following the property of line-symmetric mechanism in Eq. (22), there is a corresponding relationship between angular displacements θ_1, θ_2, θ_3 and θ_4, θ_5, θ_6. In addition, for each motion branch, the sign in Eq. (22) is listed in Table 1. The

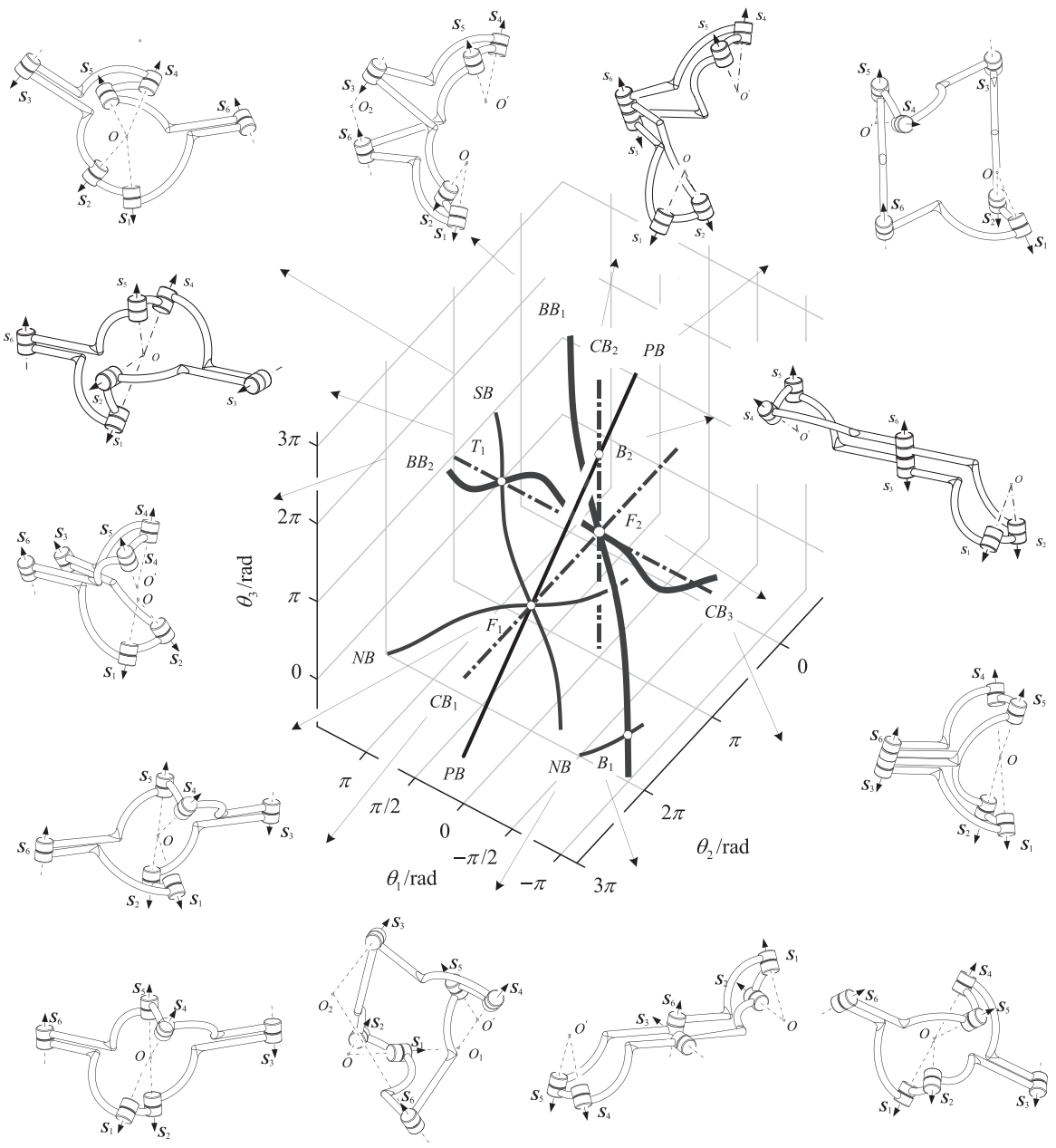

Fig. 13. Kinematic curves, furcation points, motion branches transformation and corresponding configurations.

kinematic curve of angular displacements θ_1, θ_2 and θ_3 is generated by using the geometric constraint of each motion branch in Matlab and eight corresponding curves are obtained as shown in Fig. 13.

The kinematic curve of the first Bricard motion branch, marked as BB_1 in the figure, is drawn by the geometric constraint in Eqs. (22), (32) and (37). The kinematic curve of the second Bricard motion branch BB_2 is drawn by the geometric constraint in Eqs. (22), (32) and (38). The kinematic curve of the planar-motion branch *PB* is drawn by the geometric constraint in Eqs. (22), (28) and (39). The kinematic curve of the spherical-motion branch *SB* is drawn by the geometric constraint in Eqs. (22), (29) and (42). The kinematic curve of the Bennett-motion branch *NB* is drawn by the geometric constraint in Eqs. (22), (31) and (46). The kinematic curve of the motion branch with joints 2 and 5 coaxial CB_1 is drawn by the geometric constraint in Eqs. (22), (28) and (47). The kinematic curve of the motion branch with joints 3 and 6 coaxial CB_2 is drawn by the geometric constraint in Eqs. (22), (28) and (48). The kinematic curve of the motion branch with joints 1 and 4 coaxial CB_3 is drawn by the geometric constraint in Eqs. (22), (29) and (49).

The intersections of the curves in Fig. 13 are known as the furcation points of the 6R metamorphic mechanism. In the figure, the curves of the first Bricard motion branch BB_1 and the Bennett-motion branch *NB* intersect at the bifurcation

Table 2
Furcation point and restricted condition for eight motion branches.

Motion branch	Furcation point	Restricted condition ($k \in \mathbf{Z}$)
BB_1	B_1, F_2	–
BB_2	T_1, F_2	–
PB	B_2, F_1	$\theta_1 = -\theta_4 = 2k\pi$
SB	T_1, F_1	$\theta_3 = -\theta_6 = (2k\pm1)\pi$
NB	B_1, F_1	$\theta_2 = -\theta_5 = 2k\pi$
CB_1	F_1, F_2	$\theta_1 = \theta_4 = 2k\pi$, $\theta_3 = \theta_6 = (2k\pm1)\pi$
CB_2	B_2, F_2	$\theta_1 = \theta_4 = 2k\pi$, $\theta_2 = \theta_5 = (2k+1)\pi$
CB_3	T_1, F_2	$\theta_2 = \theta_3 = \theta_4 = \theta_5 = (2k+1)\pi$

point B_1. The curves of the planar-motion branch PB and the motion branch with joints 3 and 6 coaxial CB_2 intersect at the bifurcation point B_2. The curves of the second Bricard motion branch BB_2, the spherical-motion branch PB and the motion branch with joints 1 and 4 coaxial CB_3 intersect at the trifurcation point T_1. The curves of the planar-motion branch PB, the spherical-motion branch SB, the Bennett-motion branch NB and the motion branch with joints 2 and 5 coaxial CB_1 intersect at the multi-furcation point F_1. The curves of the first Bricard motion branch BB_1, the second Bricard motion branch BB_2, the motion branch with joints 2 and 5 coaxial CB_1, the motion branch with joints 3 and 6 coaxial CB_2 and the motion branch with joints 1 and 4 coaxial CB_3 intersect at the multi-furcation point F_2. The coordinates of these five furcation points are identical with the solutions to geometric constraint equations before.

Fig. 13 also gives the corresponding configurations of eight motion branches and five furcation points. The motion transition are reflected in the kinematic curve. We excite the motion branch in practice at a singular position by exerting geometric constraints at corresponding joints. The metamorphic mechanism will run into a planar 4R motion branch PB at the bifurcation point B_2 or multi-furcation point F_1 under the restricted condition $\theta_1 = -\theta_4 = 2k\pi$ ($k \in \mathbf{Z}$). The mechanism will run into a spherical 4R motion branch SB at the trifurcation point T_1 or multi-furcation point F_1 under the restricted condition $\theta_3 = -\theta_6 = (2k\pm1)\pi$. The mechanism will also run into Bennett-motion branch NB at the bifurcation point B_1 or multi-furcation point F_1 under the restricted condition $\theta_2 = -\theta_5 = 2k\pi$, and into the motion branch CB_1 with joints 2 and 5 being coaxial at the multi-furcation point F_1 or F_2 under the restricted condition $\theta_1 = \theta_4 = 2k\pi$ and $\theta_3 = \theta_6 = (2k\pm1)\pi$. More variety of the branches include the motion branch CB_2 with joints 3 and 6 being coaxial at the bifurcation point B_2 or multi-furcation point F_2 under the restricted condition $\theta_1 = \theta_4 = 2k\pi$ and $\theta_2 = \theta_5 = (2k+1)\pi$, the motion branch CB_3 with joints 1 and 4 being coaxial at the trifurcation point T_1 or multi-furcation point F_2 under the restricted condition $\theta_2 = \theta_3 = \theta_4 = \theta_5 = (2k+1)\pi$. All variety of conditions are summarized in Table 2.

6. Conclusion

This paper used the analysis of the distance between two points and the angle between two joints that give the closeness measure of two common parpendiculars to develop a novel 6R metamorphic mechanism with eight motion branches with multiple furcation points. Based on the Bennett mechanism, when the distance of two points is zero indicating two common parpendiculars coincide, and when two axes of the opposite joints are parallel, by adding two revolute joints, a 6R metamorphic mechanism is produced with eight motion branches. The reconfiguration will occur at a trifurcation point, two mulfifurcation points, and two bifurcation points of this novel 6R metamorphic mechanism.

As the joint condition of a mechanism is constrained by the closure equation, and when two joints are geometrically constrained or unconstrained, the mechanism forms different motion branches. The novel 6R metamorphic mechanism presented has been proved to have two 6R motion branches when no joints are geometrically constrained. During motion, when two joints are geometrically constrained, there are three 4R motion branches as the planar-motion branch, the spherical-motion branch and the Bennett-motion branch. Further, when four joints are geometrically constrained, three motion branches with coaxial joints are presented.

All motion screws of the 6R metamorphic mechanism have their geometry morphologies. When the 6R metamorphic mechanism is under different motion branches, geometry morphology of the screws varies. Constrained by the closure equation, geometry morphologies of the novel 6R metamorphic mechanism are obtained. Different geometry morphologies were provided for corresponding motion branches. The two 6R motion branches form two different geometry morphologies of screw system of the fifth order. The three 4R motion branches form three different geometry morphologies of screw system of the third order. Thus, the 6R metamorphic mechanism can accomplish the transformation between different screw systems.

Acknowledgements

The authors acknowledge the support of the National Natural Science Foundation of China (Project no. 51535008, 51721003) and the Engineering and Physical Sciences Research Council of United Kingdom (Project no. EP/P026087/1, EP/S019790/1) and the International Collaboration Scheme under Grant no. B16034.

Appendix A: Elements of the closure equation

$$\cos\theta_1\cos\theta_2\cos\theta_3-\cos\theta_1\sin\theta_2\sin\theta_3-\frac{\sqrt{2}}{2}\sin\theta_1\sin\theta_2\cos\theta_3-\frac{\sqrt{2}}{2}\sin\theta_1\cos\theta_2\sin\theta_3$$
$$=\cos\theta_4\cos\theta_5\cos\theta_6-\frac{\sqrt{2}}{2}\sin\theta_4\sin\theta_5\cos\theta_6-\cos\theta_4\sin\theta_5\sin\theta_6-\frac{\sqrt{2}}{2}\sin\theta_4\cos\theta_5\sin\theta_6 \tag{A1}$$

$$\sin\theta_1\cos\theta_2\cos\theta_3-\sin\theta_1\sin\theta_2\sin\theta_3+\frac{\sqrt{2}}{2}\cos\theta_1\sin\theta_2\cos\theta_3+\frac{\sqrt{2}}{2}\cos\theta_1\cos\theta_2\sin\theta_3$$
$$=\frac{\sqrt{2}}{2}\cos\theta_4\cos\theta_5\sin\theta_6-\frac{1}{2}\sin\theta_4\sin\theta_5\sin\theta_6+\frac{\sqrt{2}}{2}\cos\theta_4\sin\theta_5\cos\theta_6+\frac{1}{2}\sin\theta_4\cos\theta_5\cos\theta_6+\frac{1}{2}\sin\theta_4 \tag{A2}$$

$$\frac{\sqrt{2}}{2}\sin\theta_2\cos\theta_3+\frac{\sqrt{2}}{2}\cos\theta_2\sin\theta_3$$
$$=\frac{\sqrt{2}}{2}\cos\theta_4\cos\theta_5\sin\theta_6-\frac{1}{2}\sin\theta_4\sin\theta_5\sin\theta_6+\frac{\sqrt{2}}{2}\cos\theta_4\sin\theta_5\cos\theta_6+\frac{1}{2}\sin\theta_4\cos\theta_5\cos\theta_6-\frac{1}{2}\sin\theta_4 \tag{A3}$$

$$\frac{\sqrt{2}}{2}\cos\theta_1\cos\theta_2\sin\theta_3+\frac{\sqrt{2}}{2}\cos\theta_1\sin\theta_2\cos\theta_3-\frac{1}{2}\sin\theta_1\sin\theta_2\sin\theta_3+\frac{1}{2}\sin\theta_1\cos\theta_2\cos\theta_3+\frac{1}{2}\sin\theta_1$$
$$=\sin\theta_4\cos\theta_5\cos\theta_6+\frac{\sqrt{2}}{2}\cos\theta_4\sin\theta_5\cos\theta_6-\sin\theta_4\sin\theta_5\sin\theta_6+\frac{\sqrt{2}}{2}\cos\theta_4\cos\theta_5\sin\theta_6 \tag{A4}$$

$$\frac{\sqrt{2}}{2}\sin\theta_1\cos\theta_2\sin\theta_3+\frac{\sqrt{2}}{2}\sin\theta_1\sin\theta_2\cos\theta_3+\frac{1}{2}\cos\theta_1\sin\theta_2\sin\theta_3-\frac{1}{2}\cos\theta_1\cos\theta_2\cos\theta_3-\frac{1}{2}\cos\theta_1$$
$$=\frac{\sqrt{2}}{2}\sin\theta_4\cos\theta_5\sin\theta_6+\frac{1}{2}\cos\theta_4\sin\theta_5\sin\theta_6+\frac{\sqrt{2}}{2}\sin\theta_4\sin\theta_5\cos\theta_6-\frac{1}{2}\cos\theta_4\cos\theta_5\cos\theta_6-\frac{1}{2}\cos\theta_4 \tag{A5}$$

$$\frac{1}{2}\sin\theta_2\sin\theta_3-\frac{1}{2}\cos\theta_2\cos\theta_3+\frac{1}{2}$$
$$=\frac{\sqrt{2}}{2}\sin\theta_4\cos\theta_5\sin\theta_6+\frac{1}{2}\cos\theta_4\sin\theta_5\sin\theta_6+\frac{\sqrt{2}}{2}\sin\theta_4\sin\theta_5\cos\theta_6-\frac{1}{2}\cos\theta_4\cos\theta_5\cos\theta_6+\frac{1}{2}\cos\theta_4 \tag{A6}$$

$$\frac{\sqrt{2}}{2}\cos\theta_1\cos\theta_2\sin\theta_3+\frac{\sqrt{2}}{2}\cos\theta_1\sin\theta_2\cos\theta_3-\frac{1}{2}\sin\theta_1\sin\theta_2\sin\theta_3+\frac{1}{2}\sin\theta_1\cos\theta_2\cos\theta_3-\frac{1}{2}\sin\theta_1$$
$$=\frac{\sqrt{2}}{2}\sin\theta_5\cos\theta_6+\frac{\sqrt{2}}{2}\cos\theta_5\sin\theta_6 \tag{A7}$$

$$\frac{\sqrt{2}}{2}\sin\theta_1\cos\theta_2\sin\theta_3+\frac{\sqrt{2}}{2}\sin\theta_1\sin\theta_2\cos\theta_3+\frac{1}{2}\cos\theta_1\sin\theta_2\sin\theta_3-\frac{1}{2}\cos\theta_1\cos\theta_2\cos\theta_3+\frac{1}{2}\cos\theta_1$$
$$=\frac{1}{2}\sin\theta_5\sin\theta_6-\frac{1}{2}\cos\theta_5\cos\theta_6+\frac{1}{2} \tag{A8}$$

$$\frac{1}{2}\sin\theta_2\sin\theta_3-\frac{1}{2}\cos\theta_2\cos\theta_3-\frac{1}{2}=\frac{1}{2}\sin\theta_5\sin\theta_6-\frac{1}{2}\cos\theta_5\cos\theta_6-\frac{1}{2} \tag{A9}$$

$$l\cos\theta_1\cos\theta_2+l\cos\theta_1(\cos\theta_2\cos\theta_3-\sin\theta_2\sin\theta_3)-\frac{\sqrt{2}}{2}l\sin\theta_1\sin\theta_2-\frac{\sqrt{2}}{2}l\sin\theta_1(\sin\theta_2\cos\theta_3+\cos\theta_2\sin\theta_3)$$
$$=-l\cos\theta_6-l \tag{A10}$$

$$l\sin\theta_1\cos\theta_2+l\sin\theta_1(\cos\theta_2\cos\theta_3-\sin\theta_2\sin\theta_3)+\frac{\sqrt{2}}{2}l\cos\theta_1\sin\theta_2+\frac{\sqrt{2}}{2}l\cos\theta_1(\sin\theta_2\cos\theta_3+\cos\theta_2\sin\theta_3)$$
$$=-\frac{\sqrt{2}}{2}l\sin\theta_6 \tag{A11}$$

$$\frac{\sqrt{2}}{2}l\sin\theta_2+\frac{\sqrt{2}}{2}l(\sin\theta_2\cos\theta_3+\cos\theta_2\sin\theta_3)$$
$$=-\frac{\sqrt{2}}{2}l\sin\theta_6 \tag{A12}$$

Reference

[1] J.S. Dai, J. Rees Jones, Mobility in metamorphic mechanisms of foldable/erectable kinds, ASME J. Mech. Des. 121 (3) (1999) 375–382.
[2] K. Wohlhart, Kinematotropic linkages, in: Recent Advances in Robot Kinematics, Springer, Dordrecht, 1996, pp. 359–368.
[3] K. Sugimoto, J. Duffy, K. Hunt, Special configurations of spatial mechanisms and robot arms, Mech. Mach. Theory 17 (2) (1982) 119–132.

[4] J. Kieffer, Differential analysis of bifurcations and isolated singularities for robots and mechanisms, IEEE Trans. Robot. Autom. 10 (1) (1994) 1–10.
[5] D. Zlatanov, I.A. Bonev, C.M. Gosselin, Constraint singularities as C-space singularities, in: Advances in Robot Kinematics: Theory and Applications, Kluwer Academic Press, 2002, pp. 183–192.
[6] A. Müller, Higher derivatives of the kinematic mapping and some applications, Mech. Mach. Theory 76 (2014) 70–85.
[7] Y. Qin, J.S. Dai, G. Gogu, Multi-furcation in a derivative queer-square mechanism, Mech. Mach. Theory 81 (2014) 36–53.
[8] F. Aimedee, G. Gogu, J.S. Dai, C. Bouzgarrou, N. Bouton, Systematization of morphing in reconfigurable mechanisms, Mech. Mach. Theory 96 (2016) 215–224.
[9] D. Gan, J.S. Dai, Q. Liao, Mobility change in two types of metamorphic parallel mechanisms, ASME J. Mech. Robot. 1 (4) (2009) 1–9.
[10] K. Zhang, J.S. Dai, Y. Fang, Geometric constraint and mobility variation of two 3SvPSv metamorphic parallel mechanisms, ASME J. Mech. Des. 135 (1) (2013) 011001.
[11] K. Zhang, J.S. Dai, Screw-system-variation enabled reconfiguration of the Bennett plano-spherical hybrid linkage and its evolved parallel mechanism, ASME J. Mech. Des. 137 (6) (2015) 062303.
[12] C. Song, Y. Chen, I.M. Chen, A 6R linkage reconfigurable between the line-symmetric Bricard linkage and the Bennett linkage, Mech. Mach. Theory 70 (2013) 278–292.
[13] K. Zhang, J.S. Dai, A kirigami-inspired 8R linkage and its evolved overconstrained 6R linkages with the rotational symmetry of order two, ASME J. Mech. Robot. 6 (2) (2014) 021007.
[14] K. Zhang, J.S. Dai, Trifurcation of the evolved Sarrus-Motion linkage based on parametric constraints, in: Advances in Robot Kinematics, Springer, Switzerland, 2014, pp. 345–353.
[15] K. Zhang, A. Müller, J.S. Dai, A novel reconfigurable 7R linkage with multifurcation, in: Advances in Reconfigurable Mechanisms and Robots II, Springer, 2016, pp. 15–25.
[16] Y. Chen, W.H. Chai, Bifurcation of a special line and plane symmetric Bricard linkage, Mech. Mach. Theory 46 (4) (2011) 515–533.
[17] H. Feng, Y. Chen, J.S. Dai, G. Gogu, Kinematic study of the general plane-symmetric Bricard linkage and its bifurcation variations, Mech. Mach. Theory 116 (2017) 89–104.
[18] Y. Chen, Z. You, An extended Myard linkage and its derived 6R linkage, ASME J. Mech. Des. 130 (5) (2008) 052301.
[19] X. He, X. Kong, D. Chablat, Stéphane Caro, Guangbo Hao, Kinematic analysis of a single-loop reconfigurable 7R mechanism with multiple operation modes, Robotica 32 (7) (2014) 1171–1188.
[20] X. Kong, M. Pfurner, Type synthesis and reconfiguration analysis of a class of variable-DOF single-loop mechanisms, Mech. Mach. Theory 85 (2015) 116–128.
[21] M. Pfurner, Synthesis and motion analysis of a single-loop 8R-chain, 2018 International Conference on Reconfigurable Mechanisms and Robots (ReMAR), IEEE, 2018.
[22] P. López-Custodio, J.S. Dai, J.M. Rico, Branch reconfiguration of Bricard linkages based on toroids intersections: line-symmetric case, ASME J. Mech. Robot. 10 (3) (2018) 031003.
[23] P. López-Custodio, J.S. Dai, J.M. Rico, Branch reconfiguration of Bricard linkages based on toroids intersections: plane-symmetric case, ASME J. Mech. Robot. 10 (3) (2018) 031002.
[24] G.T. Bennett, A new mechanism, Engineering 76 (1903) 777.
[25] G.T. Bennett, The parallel motion of Sarrut and some allied mechanisms, Phil. Mag. Ser. 6 (9) (1905) 803–810.
[26] Kutzbach, Mechanische leitungsverzweigung, ihre gesetze und anwendungen, Maschinenbau 8 (21) (1929) 710–716.
[27] J.S. Dai, Z. Huang, H. Lipkin, Mobility of overconstrained parallel mechanisms, ASME J. Mech. Des. 128 (1) (2006) 220–229.
[28] J.S. Dai, Finite displacement screw operators with embedded Chasles' motion, ASME J. Mech. Robot. 4 (4) (2012) 041002.
[29] J.E. Baker, The Bennett, Goldberg and Myard linkages—in perspective, Mech. Mach. Theory 14 (4) (1979) 239–253.
[30] R. Bricard, Mémoire sur la théorie de l'octaèdre articulé, J. Pure Appl. Math. 3 (1897) 113–148.
[31] R. Bricard, Leçons De Cinématique, Gauthier-Villars, Paris, 1926 Tome II Cinématique Appliquée.
[32] J.E. Baker, An analysis of the Bricard linkages, Mech. Mach. Theory 15 (4) (1980) 267–286.
[33] J.S. Dai, Geometrical Foundations and Screw Algebra for Mechanisms and Robotics, Higher Education Press, Beijing, China, 2014 ISBN: 978-7-04-033483-8. (translated from J.S. Dai, Screw Algebra and Kinematic Approaches for Mechanisms and Robotics, to be published by Springer, London, 2019).